

Northumbria Research Link

Citation: Hill, Emily, Gudmundsson, Hilmar, Carr, Rachel, Stokes, Chris R. and King, Helen (2021) Twenty-first century response of Petermann Glacier, northwest Greenland to ice shelf loss. *Journal of Glaciology*, 67 (261). pp. 147-157. ISSN 0022-1430

Published by: Cambridge University Press

URL: <https://doi.org/10.1017/jog.2020.97> <<https://doi.org/10.1017/jog.2020.97>>

This version was downloaded from Northumbria Research Link:
<http://nrl.northumbria.ac.uk/id/eprint/44607/>

Northumbria University has developed Northumbria Research Link (NRL) to enable users to access the University's research output. Copyright © and moral rights for items on NRL are retained by the individual author(s) and/or other copyright owners. Single copies of full items can be reproduced, displayed or performed, and given to third parties in any format or medium for personal research or study, educational, or not-for-profit purposes without prior permission or charge, provided the authors, title and full bibliographic details are given, as well as a hyperlink and/or URL to the original metadata page. The content must not be changed in any way. Full items must not be sold commercially in any format or medium without formal permission of the copyright holder. The full policy is available online: <http://nrl.northumbria.ac.uk/policies.html>

This document may differ from the final, published version of the research and has been made available online in accordance with publisher policies. To read and/or cite from the published version of the research, please visit the publisher's website (a subscription may be required.)

21st century response of Petermann Glacier, northwest Greenland to ice shelf loss

Emily A. HILL,^{1*} G. Hilmar GUDMUNDSSON,² J. Rachel CARR,¹ Chris R. STOKES³, Helen M.
KING²

¹*School of Geography, Politics, and Sociology, Newcastle University, Newcastle-upon-Tyne, NE1 7RU, UK*

²*Department of Geography and Environmental Sciences, Northumbria University, Newcastle-upon-Tyne,
NE1 8ST, UK*

³*Department of Geography, Durham University, Durham, DH1 3LE, UK*

Correspondence: Emily Hill <emily.hill@northumbria.ac.uk>

ABSTRACT. Ice shelves restrain flow from the Greenland and Antarctic ice sheets. Climate-ocean warming could force thinning or collapse of floating ice shelves and subsequently accelerate flow, increase ice discharge, and raise global mean sea levels. Petermann Glacier (PG), northwest Greenland, recently lost large sections of its ice shelf, but its response to total ice shelf loss in the future remains uncertain. Here, we use the ice flow model Úa to assess the sensitivity of PG to changes in ice shelf extent, and to estimate the resultant loss of grounded ice and contribution to sea level rise. Our results have shown that under several scenarios of ice shelf thinning and retreat, removal of the shelf will not contribute substantially to global mean sea level (< 1 mm). We hypothesise that grounded ice loss was limited by the stabilization of the grounding line at a topographic high approximately 12 km inland of its current grounding line position. Further inland, the likelihood of a narrow fjord that slopes seawards suggests that PG is likely to remain insensitive to terminus changes in the near future.

*Present address: Department of Geography and Environmental Sciences, Northumbria University, Newcastle-upon-Tyne, NE1 8ST, UK UK.

25 **INTRODUCTION**

26 Fast-flowing outlet glaciers draining the Greenland Ice Sheet are dynamically coupled to changes at their
27 terminus (Nick and others, 2009). Many outlet glaciers have thinned and accelerated in response to 21st
28 century terminus retreat from either a grounded (e.g. Howat and others, 2007; Joughin and others, 2008;
29 Moon and others, 2012) or floating terminus (Joughin and others, 2008; Hill and others, 2017). Laterally
30 confined ice shelves at marine termini can provide strong back-stress (i.e. buttressing) on grounded ice
31 (Schoof and others, 2017; Haseloff and Sergienko, 2018). However, floating ice shelves could be destabilised
32 under future climate-ocean warming, reducing resistive stress at the grounding line, which in turn could
33 accelerate ice flow, increase ice discharge, and ultimately raise global mean sea level. Ice shelf buttressing
34 has been the focus of recent work on ice shelf collapse/stability in Antarctica (e.g. De Rydt and others,
35 2015; Paolo and others, 2015; Reese and others, 2018a), but has received limited attention in Greenland.

36 Petermann Glacier (PG) is a fast flowing ($\sim 1 \text{ km yr}^{-1}$) outlet glacier in northwest Greenland that
37 drains approximately 4% of the ice sheet (Figure 1: Münchow and others, 2014). The catchment contains
38 $1.6 \times 10^5 \text{ km}^3$ of ice volume above flotation (VAF), equivalent to 0.41 m of global mean sea level rise.
39 PG terminates in one of the last remaining ice shelves in Greenland (Hill and others, 2017) (Petermann
40 Glacier Ice Shelf: hereafter PGIS). In the early Holocene the grounding line retreated from the mouth of
41 the fjord (Jakobsson and others, 2018), but the extent of the ice shelf remained largely unchanged. More
42 recently, two large well-documented calving events in 2010 and 2012 (Nick and others, 2012; Johannessen
43 and others, 2013; Münchow and others, 2014) shortened the ice shelf from $\sim 70 \text{ km}$ to 46 km (Figure 1),
44 which caused some inland ice acceleration ($\sim 12\%$) after 2012 (Münchow and others, 2016; Rückamp and
45 others, 2019). Aside from this, Petermann Glacier does not appear to be undergoing significant temporal
46 changes in geometry or speed as it has exhibited limited surface lowering (Figure 2), no obvious grounding
47 line retreat over a 19-year period (1992–2011: Hogg and others, 2016), and no significant speed-up in
48 response to recent calving (Nick and others, 2010; Rückamp and others, 2019).

49 Alongside episodic calving, the extent of the PGIS is controlled by ice-ocean interactions that force
50 high basal melt rates ($\sim 35 \text{ m yr}^{-1}$) beneath the shelf (Rignot and Steffen, 2008). Indeed melting along
51 the base of the ice shelf is considered to account for $\sim 80\%$ of mass loss from the PGIS (Rignot and others,
52 2008; Münchow and others, 2014). Recent warming ($\sim 0.2^\circ\text{C}$) of Atlantic water between 2002 and 2016
53 (Münchow and others, 2011; Washam and others, 2018), accompanied by stronger ocean circulation and

54 the break up of sea ice, are likely to have promoted warm water transport into the Petermann fjord and
 55 beneath the ice shelf (Johnson and others, 2011; Shroyer and others, 2017; Washam and others, 2018). In
 56 response to recent ocean warming and increased subglacial discharge, basal melt rates are estimated to have
 57 increased by 8.1 m yr^{-1} from the 1990s to early 2000s (Cai and others, 2017). The most recent estimates
 58 revealed 50 m yr^{-1} of basal melt at the grounding line between 2011 and 2015 (Wilson and others, 2017).

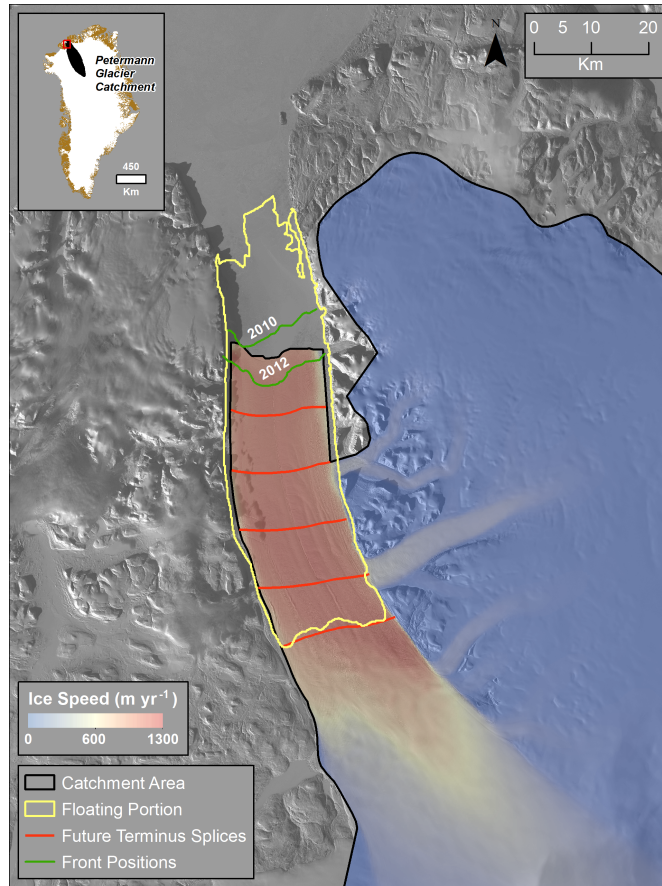


Fig. 1. Study figure of Petermann Glacier, northwest Greenland. The yellow outline shows the former extent of PGIS prior to calving events in 2010 and 2012 which are shown in green. Splices of the ice shelf removed during our model experiments are shown in red. The glacier catchment, i.e. our model domain, is outlined in black. Note that the terminus re-advanced following the 2012 calving event. Ice flow speeds are derived from the MEaSUREs Greenland annual ice sheet velocity mosaic (Joughin and others, 2010b) supplied courtesy of the NASA National Snow and Ice Data Center. Background imagery is panchromatic band 8 (15 m resolution) Landsat 8 imagery from winter 2016, acquired from the U.S. Geological Survey Earth Explorer.

59 Reductions in the extent and/or thickness of the PGIS in future could reduce buttressing at the ground-
 60 ing line and accelerate ice flow. Accelerated ice flow has been documented following ice shelf thinning or

collapse both across Antarctica (Antarctic Peninsula: Scambos and others (2004); De Rydt and others (2015), Amundsen Sea region: Rignot and others (2014); Gudmundsson and others (2019), and in East Antarctica Miles and others (2018)) and Greenland (Jakobshavn Isbræ: Joughin and others (2004, 2008) and Zachariæ Isstrøm: Mougnot and others (2015)). It is therefore important to quantify the impact of losing the PGIS on future ice discharge and sea level rise. Previous work used a flowline model at PG to examine both the short term response to ice shelf collapse (Nick and others, 2012), and the long-term sea level rise contribution under scenarios of future climate change (Nick and others, 2013). However, one-dimensional (1HD) models do not account for lateral stresses and buttressing in both horizontal directions which limits the accuracy of sea level rise projections (Gudmundsson, 2013; Bondzio and others, 2017). More recently, Hill and others (2018b) used a two-dimensional (2HD) ice flow model $\acute{U}a$ (Gudmundsson and others, 2012), to examine the time-independent response of PG to large calving events. While this showed ice shelf collapse could cause a 96% instantaneous speed-up, it did not examine the transient response of PG to a loss of ice-shelf buttressing. Thus, aside from using a flowline model (Nick and others, 2012), no modelling study has yet assessed the impact of ice shelf thinning/collapse on PG's future contribution to sea level rise.

Here, we use $\acute{U}a$ to assess the long-term (100-yr) dynamic response and sea level contribution of PG to changes downstream of the grounding line. To do this, we perform four forward-in-time sensitivity experiments to assess the future evolution of PG under different scenarios of ice shelf change. The first represents a continuation of current conditions with no further change in ice shelf extent (control run). The following experiments were then designed to encompass the main mass loss mechanisms for the PGIS. The second raised basal melt rates but left the terminus position fixed through time. The following two experiments both impose enhanced basal melting but simulate two mechanisms of ice shelf loss. The third experiment episodically removes sections of the shelf, similar in size to past observed calving events, and the final experiment imposes immediate ice shelf collapse.

METHODS

Model set-up

$\acute{U}a$ (Gudmundsson, 2020) is a vertically integrated ice flow model that solves the ice dynamics equations using the shallow ice-stream/shelf approximation (SSA) (Morland, 1987; MacAyeal, 1989), a Weertman-sliding law (Weertman, 1957), and Glen's flow law (Glen, 1955). The model has been used to understand

90 grounding line dynamics (Pattyn and others, 2012; Gudmundsson and others, 2012) and the impact of ice
91 shelf buttressing and collapse on outlet glacier dynamics in both Antarctica (De Rydt and others, 2015;
92 Reese and others, 2018a) and Greenland (e.g. Hill and others, 2018b).

93 To set-up the model we use 150 m resolution bedrock geometry, fjord bathymetry, ice thickness, and
94 surface topography from the BedMachine v3 dataset (Morlighem and others, 2017). The model domain
95 extends from the ice shelf front in 2016 across the ice surface drainage catchment of PG ($\sim 85,000$ km²:
96 Figure 1). Our entire computational domain can be seen in Figure 1 and in Figure S1. We used the *Mesh2D*
97 Delaunay-based unstructured mesh-generator (Engwirda, 2014) to create a linear triangular finite-element
98 mesh with 111391 elements and 56340 nodes (Figure S1). The mesh was refined anisotropically based on
99 three criteria: i) flotation mask, ii) measured flow speeds, and iii) surface elevation. Element sizes were
100 ~ 0.3 km across the ice tongue, where flow speeds are >250 m yr⁻¹, and at ice surface elevations <750
101 m a.s.l.. Where flow speeds are <10 m yr⁻¹ and surface elevation exceeds 1200 m a.s.l., element sizes
102 reached a maximum of 15 km. Nunataks on the eastern side of PGIS were digitized in 2016 Landsat-8
103 imagery and treated as holes within the mesh, along the boundary of which we fix velocity to zero in both
104 normal and tangential directions. Topographic parameters (ice surface, thickness, and bed topography)
105 were linearly interpolated onto this mesh. The boundary condition along the floating ice shelf terminus
106 is hydrostatic ocean pressure in the normal direction, and free-slip in the tangential. Along the inland
107 catchment boundary we used a fixed (no-slip in normal or tangential directions) zero velocity condition
108 to conserve mass within our model domain. Velocities were also fixed to zero along the lateral ice shelf
109 margins (excluding along the fronts of glaciers on the eastern side of the fjord) as this optimally replicates
110 lateral stresses and ice flow along the PGIS (see Hill and others, 2018b).

111 We used inverse methodology to initialize the model. Initial observed velocities were taken from the
112 2016/17 MEaSUREs Greenland annual ice sheet velocity mosaic (Joughin and others, 2010b) derived from
113 both optical (Landsat-8) and synthetic aperture radar data (TerraSAR-X, TanDEM-X, Sentinel-1A and
114 1B). We optimized our model to observed velocities by simultaneously estimating the basal slipperiness
115 parameter (C) in the Weertman sliding law and the ice rheology parameter (A) in Glen's flow law (see
116 Figure S2). The stress exponents in the Weertman sliding law (m) and Glen's flow law (n) were both
117 set to 3, as commonly used in glaciological studies. This same inverse methodology and model has now
118 been used in a number of previous studies (Gudmundsson and others, 2019; Reese and others, 2018b; Hill
119 and others, 2018b). Inversion was done by minimizing the cost function of a misfit and regularization

120 term. $\hat{U}a$ uses the adjoint method to calculate the gradients of the cost function with respect to A and
 121 C in a computationally efficient way. Regularization of the A and C fields is imposed using Tikhonov
 122 regularization of both the amplitude and spatial gradients of A and C . We tested a series of regularization
 123 parameter values and selected final values based on an L -curve analysis. After a total of 900 iterations,
 124 the mean difference between modeled and observed velocities was 9.5 m yr^{-1} (15%). This increased to 14
 125 m yr^{-1} where speeds are $>300 \text{ m yr}^{-1}$ and to 23 m yr^{-1} along the PGIS.

Annual surface mass balance (SMB) for all experiments were input from RACMO2.3 (1-km resolution)
 (Noël and others, 2016), averaged between 2011 and 2016, to reflect current mass balance conditions. Basal
 melt rates (defined here as melting along the base of the floating shelf) at PGIS are correlated with ice
 thickness and are enhanced on either side of basal channels (Rignot and Steffen, 2008; Wilson and others,
 2017). In line with a number of studies, we parameterise melt rates based on ice thickness (Joughin and
 others, 2010a; Favier and others, 2014). Throughout our experiments basal melt rates mb at each timestep
 (t) were prescribed as a linear-function of ice thickness:

$$mb(t) = \frac{m_{\max} - m_{\min}}{h_{\max}(t) - h_{\min}(t)} \cdot h(t) \quad (1)$$

126 where the slope is determined using maximum floating ice thickness (h_{\max}) minus minimum floating ice
 127 thickness (h_{\min}) and the difference between minimum melt rates (m_{\min} : which we always set to 0 m yr^{-1})
 128 and maximum (m_{\max}) melt rates for each experiment. Initially we impose a m_{\max} of 37 m yr^{-1} to reflect
 129 near steady-state melt rates in previous studies (Rignot and Steffen, 2008; Cai and others, 2017). This
 130 reproduces the expected melt rate pattern beneath the shelf; highest at the grounding line (37 m yr^{-1})
 131 and either side of basal channels, decreasing to 1 m yr^{-1} near the terminus (Figure 2).

132 **Model initialization and control run**

133 For forward transient experiments, $\hat{U}a$ allows for a fully implicit time integration, where, at each time-step,
 134 changes in geometry, grounding line position and velocity are calculated implicitly. During each forward
 135 run, we incorporated automated adaptive time-stepping and automated time-dependent mesh refinement
 136 around the grounding line. Our adaptive time-stepping increases the timestep if the ratio between the
 137 maximum number of non-linear iterations over the previous 5 timesteps and the target number of iterations
 138 (set to 4) is less than one. We begin with a timestep of 0.01 years and set our target timestep to 1 year.
 139 Mesh refinement around the grounding line is known to improve estimates of stress distributions and

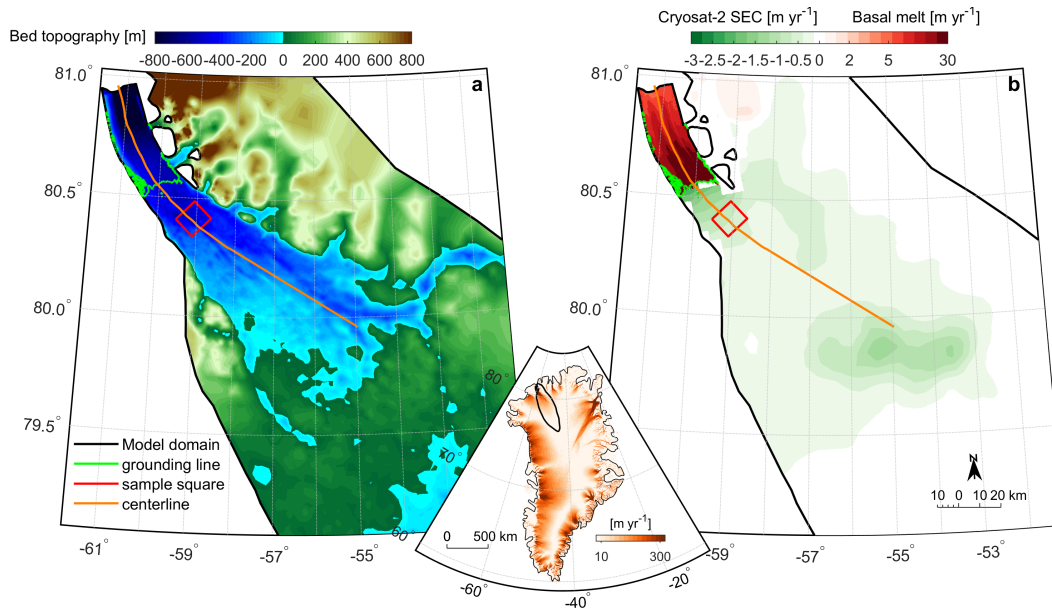


Fig. 2. a) Bed topography [m] across the lower portion of the Petermann Glacier catchment, b) is initially prescribed steady-state melt rates beneath the ice tongue (on a logarithmic scale in red) and green shading is observed surface elevation change (SEC) from Cryosat-2 between 2011 and 2016 (Simonsen and Sørensen, 2017), both of which are in m yr^{-1} . Both panels show the model domain (black line), the grounding line at the beginning of our control run (green line), glacier center profile line (orange line), and a sample area (red square) 20 km inland. This square was chosen sufficiently far inland so that it always remained grounded throughout each experiment. Inset map shows Greenland ice flow speed [m yr^{-1}] in orange and the Petermann catchment outlined in black.

140 migration rates of the grounding line (Goldberg and others, 2009; Durand and others, 2009; Pattyn and
 141 others, 2012; Schoof and others, 2017; Cornford and others, 2013). Within 2 km of the grounding line, we
 142 locally refined element sizes to 100 m. We also performed mesh sensitivity experiments, and found our
 143 results were independent of the resolution of the mesh around the grounding line (see Supplementary Text
 144 S1). In a post-processing step, and for illustrative purposes, annual width-averaged grounding line retreat
 145 was then calculated using the commonly adopted box method (see Hill and others, 2018a).

146 In addition to transient mesh refinement, we calculate the basal melt rate field at each time step to
 147 account for changes in ice thickness (h) throughout our simulations. Maximum and minimum ice thickness
 148 values are updated at each time step but m_{\max} remains constant. This approach, using the difference in ice
 149 thickness at each timestep, has the effect of keeping the range of melting across the shelf constant despite
 150 reductions in ice thickness through time. In reality this reflects a warming at shallower water depths, but
 151 in the absence of additional information on how melt rates will change through time we choose to keep the

152 range of melt rates constant in time across the shelf. Melt rates are applied to every floating and partially
 153 floating node at each time step. While applying melt rates right at the grounding line (at partially floating
 154 nodes) can overestimate mass loss (Seroussi and Morlighem, 2018) we performed a sensitivity experiment
 155 and found that this has a very limited affect on our results (see Figure S7).

Using the initial input SMB, basal melt rates ($m_{\max} = 37 \text{ m yr}^{-1}$), and estimates of basal slipperiness (C) and ice rheology parameter (A), we performed a control run. This control run was designed to reflect the future evolution of PG if melt rates remain low and no large calving events occur, but with some inland thinning ($\sim 1 \text{ m yr}^{-1}$) similar to observations (Figure 2: Simonsen and Sørensen, 2017). It was not meant to replicate steady-state conditions, i.e. total mass balance equal to zero. First, we allowed for a short period of model relaxation, as experience has shown that transient runs tend to exhibit a short period of anonymously high rates-of-change following initialization. We calculated the approximate total mass balance (M_{total}) at the beginning of this run, based on the total melt flux (M_{basal} and M_{surface}) minus the approximate calving flux (M_{calving}). This is not calculated explicitly within our model as we do not account for calving but is instead based on fixed (width \times height \times velocity) at the glacier terminus:

$$M_{\text{total}} = M_{\text{basal}} + M_{\text{surface}} - M_{\text{calving}} \quad (2)$$

156 At time 0 our estimated calving flux is 0.99 Gt a^{-1} , total melt flux is -3.2 Gt a^{-1} and total mass balance
 157 is therefore -4.19 Gt a^{-1} . Initial elevation changes were in good agreement with Cryosat 2.2 elevation
 158 changes from 2011 to 2016 (Figure 2), albeit slightly lower due to imposing near to steady-state melt rates
 159 (see Figure S4). Over the entire control run there was almost no change from our initial mass balance.
 160 These early changes in mass balance over the first 10 years are shown in Figure S6. However, some
 161 variability occurred within the first 10 years, so we discarded these as model drift and time=10 years was
 162 the starting point for all further experiments. We note that our final results are not sensitive to the selected
 163 duration of this initial relaxation period as our total modelling time is several times larger, and the changes
 164 within the first 10 years are small with respect to the total mass balance.

165 After running the model for 10 years, to account for the period of model drift, we ran our control
 166 run forward in time for 100 years, during which there was no change in melt rates or horizontal extent of
 167 the ice shelf. The terminus position is fixed through time and is not allowed to advance or retreat freely.
 168 Throughout this, the grounding line position was stable, and the flux across the grounding line (9.85 Gt
 169 a^{-1}) remained similar to observations (Wilson and others, 2017). As no perturbation in ice shelf extent

170 was imposed, thinning rates remained small (-0.17 m a^{-1}), acceleration was limited (0.26 m a^{-2} : Figures
 171 3 and 4), and the total contribution to sea level rise over 100 years was only 0.43 mm (Figure 5, Table 1).

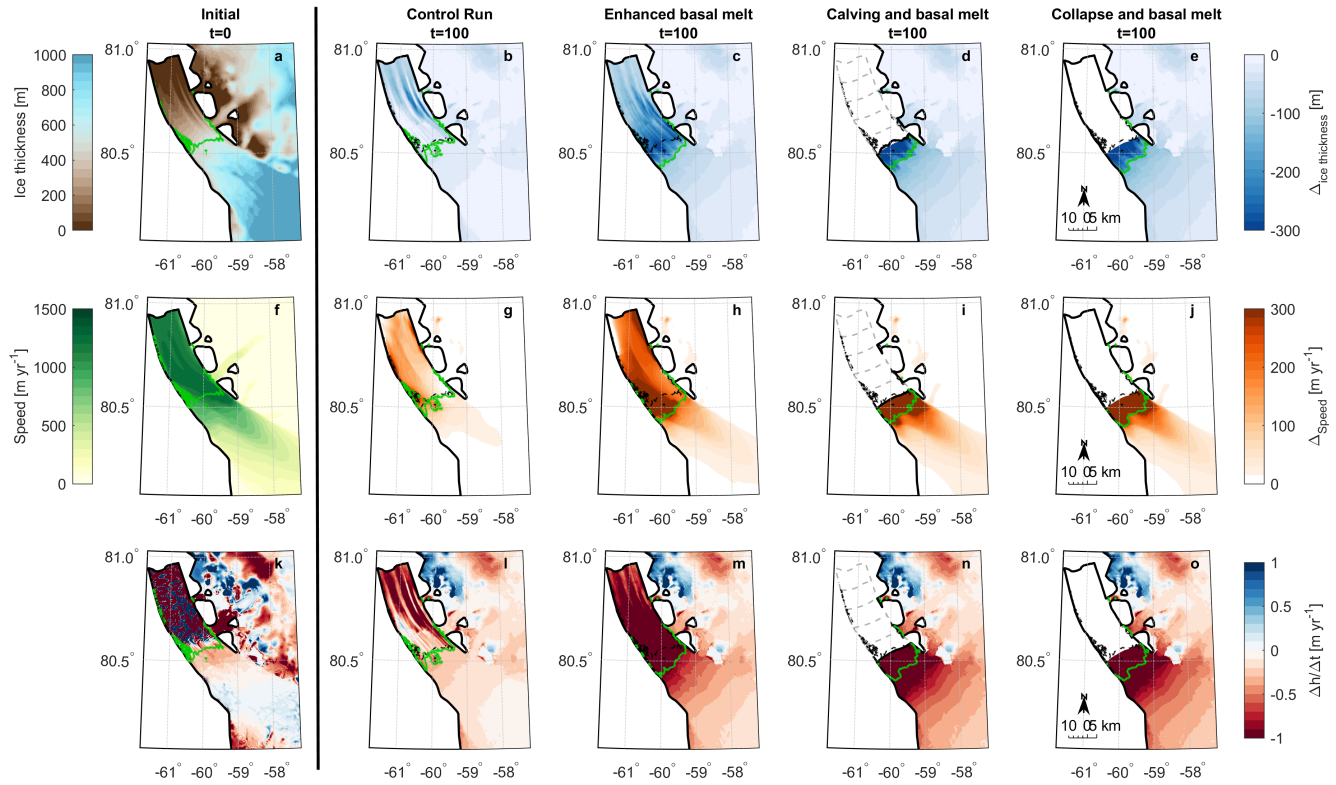


Fig. 3. Top row shows initial ice thickness [m] at time = 0 (a) and plots b-e show the change in ice thickness [m] after 100 years for each of our experiments. The middle row of plots shows initial ice speed (f) in m yr^{-1} and plots g-j show change in speed [m yr^{-1}] after 100 years. The bottom row shows initial thinning rates after the initialization period (k) in m yr^{-1} where red is thinning and blue is thickening, and plots l-o show thinning rates at the last simulation year (100 years) [m yr^{-1}]. In plots a, f and k, the green line represents the initial grounding line position. In all other plots the green line is the position of the grounding line after 100-years for each experiment. In d, i and n, the dotted lines represent calved icebergs at 5-year intervals between 5 and 25 years.

172 Experiments

173 Following our model initialization and control run, we performed three additional perturbation experiments.
 174 These experiments should not necessarily be viewed as projections but were designed to assess the sensitivity
 175 of PG to three distinct scenarios of ice shelf evolution over the next 100 years. We note that these
 176 experiments only assess the sea level rise contribution associated with ice shelf loss, as in all cases our SMB
 177 remains fixed in time. Our three experiments are:

- 178 1. Enhanced basal melt rates and no change in ice tongue extent
- 179 2. Enhanced basal melt rates together with prescribed episodic calving
- 180 3. Immediate ice shelf collapse and enhanced melt in newly floating cells

181 Each of these experiments began after the 10-year initialization period, and we ran the model forward
182 in time for 100 years. Our first experiment aims to assess the role of enhanced basal melt rates, and
183 associated thinning of the shelf but with no perturbation in horizontal ice shelf extent. At the beginning of
184 the simulation, we increased the maximum basal melt rate beneath the PGIS to $m_{\max} = 50 \text{ m yr}^{-1}$, in line
185 with the high-end of recent observational estimates (Wilson and others, 2017). This maximum melt rate
186 was then kept fixed throughout the experiment, despite changes in ice shelf thickness. It is possible that
187 ocean warming in the future may enhance melt rates further at PG, but given the uncertainties associated
188 with projecting future basal melt rates, we merely assess the impact of current melt conditions over the
189 next 100-years. As a result, these estimates likely represent the low-end member response of PG to future
190 ice tongue melt.

191 Our second experiment takes the enhanced basal melting from experiment one and additionally removed
192 five large sections of the ice tongue ($\sim 180 \text{ km}^2$) at 5-year intervals from 5–25 years (Figure 1). This assumes
193 that PG will continue to lose its ice tongue via episodic calving, similar in size to large calving events in 2010
194 and 2012 (Münchow and others, 2014). Indeed, a large rift formed in 2016 suggesting calving is imminent
195 (Münchow and others, 2016). As in experiment one, we updated the maximum melt rate to 50 m yr^{-1} at
196 the beginning of the simulation, and then at five year intervals we deactivated elements from our existing
197 mesh, downstream of the new prescribed calving front position. In between, and after these calving front
198 perturbations, we did not impose an additional calving law. Here, we aim to assess the response to current
199 ice shelf retreat and eventual collapse, and not the future evolution once the glacier calves from a grounded
200 terminus.

201 Our final experiment simulates another scenario of ice shelf loss, by removing it entirely at the beginning
202 of the simulation. Since the early 2000s, several floating ice shelves have collapsed, across both Antarctica
203 (e.g. Scambos and others, 2004) and Greenland (Hill and others, 2018a). Washam and others (2018)
204 highlighted an incised channel close to the grounding line of PG (Figure 4c). Enhanced melting within
205 this basal channel could weaken the PGIS causing it to calve in its entirety. This experiment immediately
206 removed the entire $\sim 885 \text{ km}^2$ ice shelf at the start of the experiment. After this, we did not prescribe

any further changes in ice front position, i.e. no calving law, in order to assess the longevity of the glacier response to initial ice shelf collapse. As the grounding line retreats we apply enhanced basal melt $m_{\max} = 50 \text{ m yr}^{-1}$ to newly floating nodes in the domain, in the same way as in previous experiments.

RESULTS

Role of enhanced basal melt

Our first experiment raised basal melt rates beneath the PGIS to range from 50 m yr^{-1} at the grounding line to $\sim 5 \text{ m yr}^{-1}$ near the terminus (Wilson and others, 2017). Under these high melt conditions, the ice shelf thinned by ~ 100 to 300 m (Figure 3c), accelerated by 300 m yr^{-1} (Figure 3h), and thinned by 2 m yr^{-1} close to the grounding line and either side of streamlined basal channels (Figure 3m). Greater basal melt-induced thinning of the shelf resulted in 48% more ice loss after 100 years (-233 Gt) than our control run. This is equivalent to 0.65 mm of global mean sea level rise (Table 1).

Table 1. Thickness change (dh/dt), change in speed between 0 and 100 years and annual acceleration calculated within a square upstream of the grounding line. Acceleration is relative to initial velocities after 10 year relaxation period (after 0–10 control run). Flux is average grounding line flux for 0–100 yrs. Mass loss is the ice volume above flotation lost by the end of the 100 year period.

	dh/dt	Change in speed	Acceleration	Flux	Mass loss	Total
	[m yr^{-1}]	[m yr^{-1}]	[m yr^{-2}]	[Gt yr^{-1}]	[Gt]	SLR
	0–100 yrs	0–100 yrs	0–100 yrs	0–100 yrs		[mm]
Control run	−0.17	691	0.26	9.85	157	0.43
Enhanced basal melt	−0.54	763	1.03	10.86	233	0.65
Calving & enhanced basal melt	−0.89	841	1.71	11.64	313	0.87
Collapse & enhanced basal melt	−0.92	873	1.63	11.58	333	0.92

During the first 20 years of the enhanced melt run, there was limited inland surface lowering or acceleration. However, 0.2 km of grounding line retreat led to a 24 km^2 loss of grounded area (Figure 5) and initiated positive feedbacks (e.g. acceleration, thinning and retreat) over the following 20 years. Greater thinning took place between 20 and 40 years close to the grounding line (188 m) compared to our control run (Figure 4b). Crucially, this thinning likely decreased back-stress at the grounding line, causing it to retreat rapidly (6.8 km from 20 to 40 year) and un-ground 134 km^2 of ice. Subsequently further inland ice

224 flow speeds increased by 13%, thinning rates rose to 1 m yr^{-1} , and there was a 16% increase in ice flux
225 across the grounding line (Figure 6). However, acceleration and thinning were confined to $\sim 10 \text{ km}$ inland
226 of the initial grounding line (Figures 3 and 4). Between 60 and 100 years, acceleration and thinning rates
227 decreased, and the grounding line appeared to stabilise $\sim 9 \text{ km}$ inland (Figure 5). Thus, with no further
228 perturbation of the ice shelf (i.e. no further increase in basal melt rates or fracture driven calving), PG
229 approached stable conditions (e.g. constant flow speeds and no further grounding line retreat: Figure 5)
230 after 60 years.

231 **Episodic calving and enhanced basal melt**

232 Our second experiment shows that the gradual loss of buttressing associated with gradual ice tongue
233 collapse and enhanced ice shelf thinning caused a larger stress perturbation at the grounding line than
234 enhanced basal melting alone. This led to greater inland thinning and acceleration (Figure 3j and o) and
235 a total ice volume loss of 313 Gt (Table 1). Despite greater ice loss, the contribution to global mean sea
236 level rise was still limited to 0.89 mm after 100 years (Figure 5a).

237 Consistent with earlier work (Nick and others, 2012; Hill and others, 2018b), our results show that
238 the glacier response to calving differs between removing the lower or upper portions of the PGIS. After
239 removing the first three sections of the ice shelf (at 5, 10, and 15 years), ice flow at the terminus accelerated
240 by only 5–10% in the 5 years between each calving event (Figure 4d). The grounding line simultaneously
241 retreated at 60 m yr^{-1} (total of 1.2 km), which is similar to retreat in the early stages of our basal melt
242 experiment (Figure 5c). This resulted in 46 km^2 loss of grounded area, equivalent to 0.1 mm of sea level
243 rise. However, further inland limited change took place, with only 6% flow acceleration and 0.05 m yr^{-2}
244 increase in thinning rates (Figure 5). This indicates that the glacier force balance was not significantly
245 altered by removing these sections of the shelf. In addition, the lower ice shelf includes the large fracture
246 that formed in 2016 (Münchow and others, 2016), which Rückamp and others (2019) showed is likely to
247 have already de-coupled the lower part of the shelf, causing a reduction in buttressing and some speed-up
248 after its formation.

249 Removing thicker (Figure 4) and stiffer (Figure S2) sections of the PGIS closer to the grounding line
250 caused greater loss of contact with the side-walls, and thus a larger reduction in lateral resistive stress
251 acting on grounded ice. Removing the fourth section of the shelf led to terminus acceleration of 41%,
252 which was four times the acceleration after previous calving events. Some terminus deceleration occurred

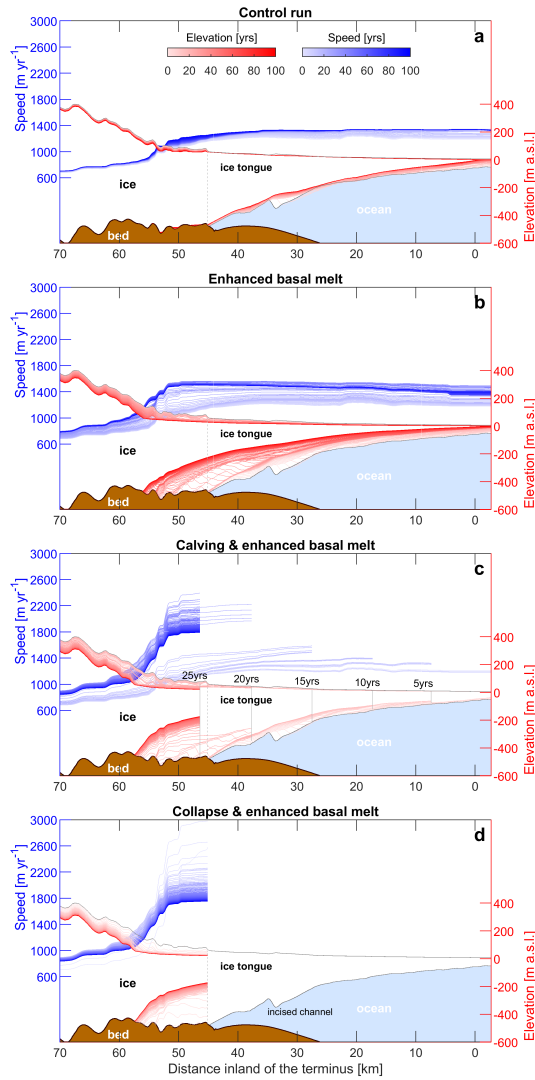


Fig. 4. Annual speed (blue) and elevation (red) along the Petermann Glacier centerline (sampled at 100 m intervals) for each of our model experiments (a–d). Pale to dark blue and pale to dark red represent each year between 0 and 100 for speed and elevation, respectively. The dotted grey line represents the initial grounding line position and the ice ocean and bed extents are from the BedMachine v3 dataset (Morlighem and others, 2017). In plot c, the grey lines are sections of the PGIS removed at 5 year intervals between 5 and 25 years.

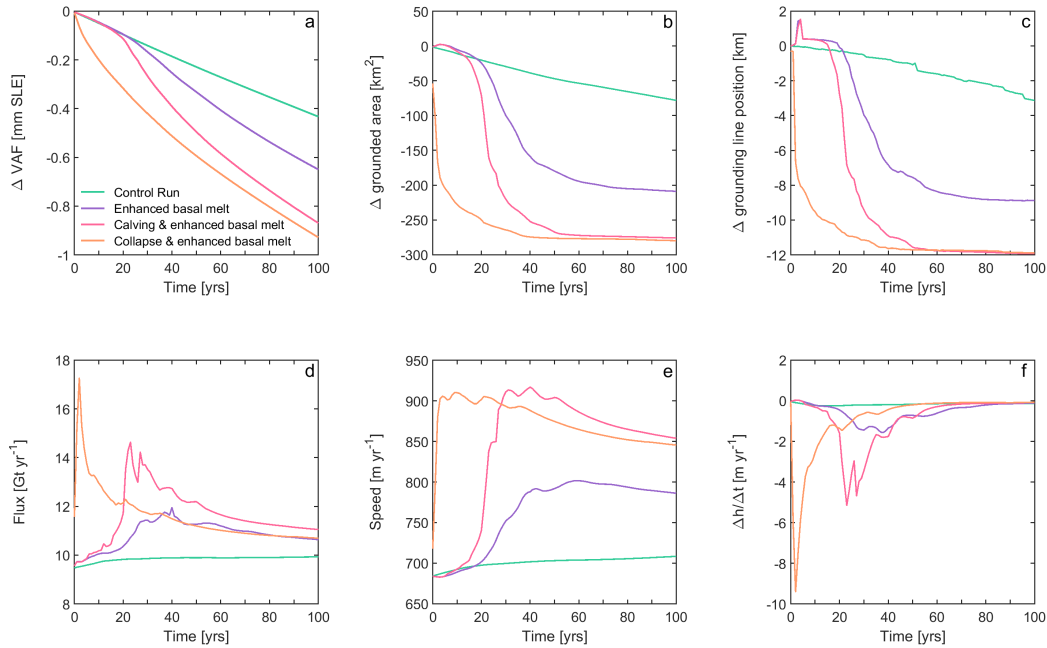


Fig. 5. Model results for each of our experiments; control run (green), enhanced basal melt (purple), prescribed calving and enhanced basal melt (pink), and ice tongue collapse and enhanced basal melt (orange). a) change in volume above flotation (VAF) in mm of global mean sea level equivalent. b) change in grounded area [km^2]. c) width-averaged grounding line retreat [km], note some advance associated with re-grounding downstream of the main grounding line position. d) annual ice flux [Gt yr^{-1}] across the grounding line. e) average annual ice flow speeds [m yr^{-1}] within a 134 km^2 square $\sim 17 \text{ km}$ inland of the grounding line (Figure 2). f) average annual thinning rates (change in thickness (h) over time (t)) in m yr^{-1} within our sample square.

253 from 23–25 years, but speeds remained high further inland (Figure 5e), and increased by a further 330 m
 254 yr^{-1} at the terminus after the final calving event. Crucially, losing these upper sections of the shelf caused
 255 the grounding line to retreat a further $\sim 8 \text{ km}$ by 30-years (Figure 5c). Retreat of the grounding line into a
 256 region of thicker ice inland led to a 240% increase in thinning rate, 25% flow acceleration, and 31% increase
 257 in ice flux during 19–30 years (Figures 3 and 5). Importantly, this period of dynamic readjustment (inland
 258 acceleration thinning and grounding line retreat) lasted ~ 10 years longer than under basal melting alone
 259 (Figure 5). However, after 70-years, PG appeared to have returned to conditions prior to the perturbation,
 260 indicated by slow deceleration (-0.67 m yr^{-2}), thinning rates returning to initial levels (-0.12 m yr^{-1}),
 261 and the grounding line stabilizing at 3 km further inland of our previous experiments (Figure 5c).

262 **Impact of immediate ice tongue collapse**

263 Our final experiment showed that if the PGIS were to instantly collapse from its current state in 2016, PG
264 would experience increased thinning and acceleration (Figure 3d, i, and n) relative to any of our previous
265 experiments but the impact of ice shelf collapse and subsequent enhanced melt would still be limited: the
266 glacier would lose about 333 Gt of ice after 100 years (Table 1). While this is more than double the ice
267 loss from our control run, and greater than removing the ice tongue episodically, it is equivalent to a global
268 mean sea level rise of only 0.92 mm (Figure 5a).

269 Our results indicate that an instant removal of the entire ice shelf in contact with the grounding
270 line appeared to cause a greater loss of buttressing than gradual sub-shelf thinning and episodic calving
271 (Experiment 2). This was evident in the first 5 years where the grounding line retreated 8.2 km (Figure
272 5c), and there was a near instantaneous increase in ice flux across the grounding line reaching a maximum
273 of 17 Gt yr⁻¹ at year three (Figure 5d). Substantial surface lowering (31 m) and a 116% (+1380 m yr⁻¹)
274 increase in flow speed at the terminus indicates a loss of back-stress (Figure 4d). Changes at the terminus
275 propagated inland, where thinning rates increased 5 fold (averaging 5.8 m yr⁻¹) and speeds increased
276 to ~900 m yr⁻¹ (+33%) over the first 5 years (from our upstream sample square: Figure 5). After the
277 initial period of acceleration, increased ice flux, and rapid retreat of the grounding line (0 to 10 years),
278 PG appeared to dynamically adjust to the loss of buttressing. Between 10 and 35 years, grounding line
279 retreat slowed to 0.08 km yr⁻¹ and ice flux decreased to 11.7 Gt yr⁻¹. During this period ice flow speeds
280 and thinning rates further inland subsided, indicating a reduction in glacier driving stress (Figure 5d).
281 After 35 years the grounding line occupied a similar position as it did after 50 years in our episodic calving
282 experiment, and remained stable for the remaining 65 years.

283 **DISCUSSION**

284 Our modelling experiments show that future changes in the extent of the PGIS (via melt only, calving,
285 or entire collapse) can cause thinning, acceleration and grounding line retreat. Of our three scenarios
286 of ice shelf loss, immediate collapse and enhanced basal melting (up to 50 m yr⁻¹) as the grounding
287 line retreats, appeared to cause the greatest loss of buttressing and led to a doubling of the sea level
288 rise contribution from 0.43 mm (if current conditions are maintained) to 0.92 mm after 100 years (Table
289 1). Immediate thinning and acceleration after shelf collapse is consistent with the observed behaviour of

290 Jakobshavn Isbræ (Thomas, 2004; Joughin and others, 2004) and Zachariæ Isstrøm (Mouginot and others,
291 2015; Hill and others, 2018a) in Greenland, and glacier acceleration following the Larsen B ice shelf collapse
292 in Antarctica (Scambos and others, 2004; De Rydt and others, 2015). However, despite this, PG appeared
293 to adjust to the loss of buttressing after ~ 40 years, after which there was limited grounding line retreat,
294 and without an increase in calving after future collapse the shelf may regrow (Nick and others, 2012). We
295 do not assess that here, but suggest it warrants further investigation. Our other experiments (melt only,
296 and prescribed calving) were able to prolong the dynamic glacier response up to ~ 60 years. However, the
297 response to basal melt alone was relatively muted (0.65 mm of sea level rise), primarily due to leaving the
298 calving front position fixed, whereas in reality sub-shelf thinning is likely to act as a precursor to calving
299 (Münchow and others, 2014). While episodic calving of the PGIS (particularly closer to the grounding line)
300 in combination with sub-shelf thinning, caused 0.87 mm of sea level rise, this remains less than immediate
301 collapse, as PG likely had time between calving events to readjust to stress imbalances.

302 Despite some dynamic change at PG, the global impact on sea level rise remains limited. Hence, the
303 key conclusion from these experiments is that, in all cases, ice tongue perturbations were unable to force
304 long-term instability of PG, i.e. irreversible thinning, acceleration, and grounding line retreat. We attribute
305 this insensitivity primarily to a stabilization of the grounding line. In all experiments the grounding line
306 positions retreated to within 3 km of each other (Figures 5c and S3). Crucially, this stabilization limits the
307 sea level rise contribution of PG to <1 mm over the next 100 years. This is much smaller than projections
308 from Jakobshavn Isbræ (2.77–5.7 mm) by 2100 (Bondzio and others, 2017; Guo and others, 2019) and
309 Zachariæ Isstrøm (up to 16 mm in an extreme case: Choi and others, 2017) but is similar to the lowest
310 emissions scenario (A1B) projections at Petermann and Kangerdlugssuaq (~ 1 mm: Nick and others, 2013).
311 We now discuss several factors limiting grounding-line migration and ice loss. These are: i) bed topography,
312 ii) lateral confinement/ fjord width, iii) fixed terminus position, and iv) basal slipperiness.

313 Bed slope is known to impact stability of glacier grounding lines (Schoof, 2007; Choi and others, 2017)
314 in the absence of additional buttressing from the lateral margins (Gudmundsson and others, 2012; Haseloff
315 and Sergienko, 2018). Initial retreat of PG's grounding line was over a shallow retrograde slope 8 km
316 inland (-0.39° : Figure 6a). In all of our experiments we observed a slowdown in grounding line retreat
317 after 50 years (Figure 5c). This is partly due to the absence of additional forcing, but also due to the
318 transition to a steeper seaward sloping ($+0.7^\circ$) portion of the bed inland ($\sim 42 - 50$ km inland on Figure
319 6a). It is likely that this prograde slope forced the grounding line to stabilize at this position. This is

320 consistent with the observed stability of grounding lines on prograde bed slopes in west Greenland (Catania
321 and others, 2018), and the role of bed topography on the retreat of glacier termini elsewhere in Greenland
322 (Bunce and others, 2018; Brough and others, 2019). At PG, a seaward sloping bed topography is likely
323 to have been a key control that, limited past grounding line retreat (Hogg and others, 2016). In addition,
324 previous modelling experiments have also shown that basal topography may limit 21st century grounding
325 line retreat (Nick and others, 2013). Elsewhere in Greenland, deep bed topography has allowed runaway
326 grounding line retreat after ice shelf collapse. For example, the collapse of Jakobshavn Isbræ's ice shelf was
327 followed by grounding line retreat and acceleration (Joughin and others, 2008, 2014), which is projected to
328 continue throughout the 21st century due to deep bed topography further inland (Guo and others, 2019;
329 Bondzio and others, 2017). Similarly, at Zachariæ Isstrøm, collapse of the ice shelf by 2012 was followed
330 by acceleration, thinning and grounding line retreat down a retrograde bedslope (Mouginot and others,
331 2015; Hill and others, 2018a). It is also projected to undergo unstable retreat of the grounding line \sim 30
332 km inland by 2100 and contribute at least 1.7 mm to sea level rise (Choi and others, 2017). However,
333 PG appears unlikely to undergo rapid unstable retreat associated with marine ice sheet instability as
334 suggested for regions of West Antarctica (e.g. Favier and others, 2014). Instead, PG is likely to behave
335 more similarly to the projected response of 79 North Glacier. Here, Choi and others (2017) showed that
336 substantial grounding line retreat, and thus sea level rise contribution (1.12 mm by 2100) will be prevented
337 by a stabilisation of the grounding line at a step in bed topography. Thus, the absence of retrograde bed
338 topography at PG suggests that it is also unlikely to undergo unstable retreat over the next 100 years.

339 In addition to the role of bed topography, channel width can also modulate grounding line retreat
340 (Jamieson and others, 2012; Åkesson and others, 2018), and has been identified as a key control on the
341 retreat of numerous glaciers using both modern (e.g. Carr and others, 2014; Steiger and others, 2017;
342 Catania and others, 2018) and palaeo records (Stokes and others, 2014; Jamieson and others, 2014). PGIS
343 is well-confined within its narrow fjord, and hence, its collapse leads to a loss of lateral resistive forces and
344 buttressing. Indeed, our results showed inland acceleration and thinning (Figures 4 and 5) following ice
345 shelf collapse, which is indicative of a loss of resistive stress at the grounding line. This behaviour contrasts
346 with observations elsewhere in northern Greenland e.g. C H. Ostenfeld Glacier. Here, collapse of a laterally
347 unconfined ice shelf did not lead to inland acceleration, which indicates that the ice shelf provided limited
348 buttressing at the grounding line (Hill and others, 2018a). Importantly, once PG's grounding line has
349 initially retreated in response to an ice tongue perturbation, the fjord width further inland does not vary

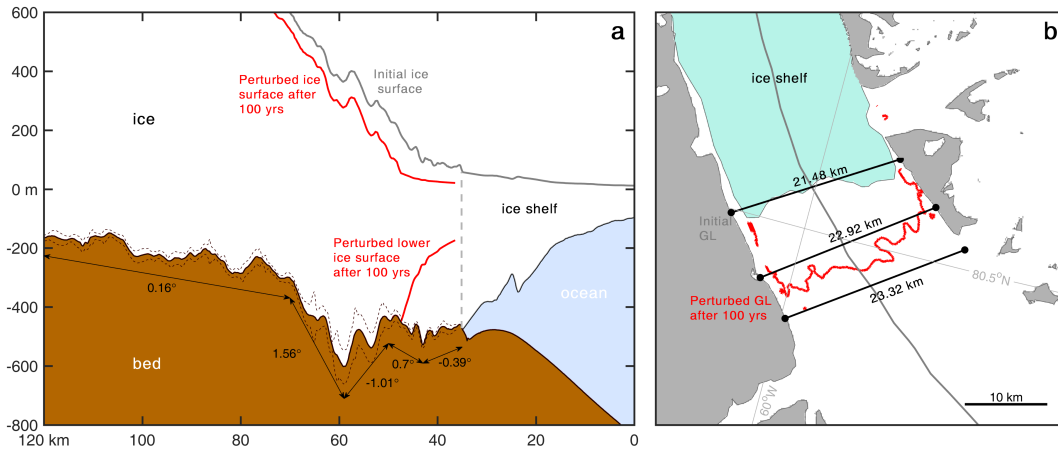


Fig. 6. a) Centerline profile (shown in grey on b) of ice surface and bed topography of Petermann Glacier. Dashed brown lines show the errors in bed topography extracted along the profile from the BedMachine v3 dataset (Morlighem and others, 2017). Annotated numbers along this profile are the degree of the bed slope between the arrows. We note that the errors in bed topography are small, and do not effect the direction and steepness of the slope along the profile. b) Plan view of the grounding line region of Petermann Glacier, displaying fjord widths at several locations: at the initial grounding line position, at the final grounding line position after 100 years in our third perturbation experiment, and further inland. We note that there is little change in fjord width between these locations.

350 substantially (< 1 km: Figure 6b). Hence, it is likely that while the grounding line retreated, there was no
 351 significant reduction in lateral drag, which in turn prevented a positive feedback of continued grounding
 352 line retreat.

353 Alongside glacier geometry (bed topography and fjord width) we acknowledge that there are additional
 354 factors that may have controlled the final grounding line position. First, in all of our simulations and
 355 aside from our prescribed calving front position in experiment three, the terminus position is fixed. It
 356 is therefore possible that in the absence of additional forcing, (e.g. continuous calving at the grounding
 357 line after ice shelf collapse), the glacier readjusted and became stable at the new grounding line position.
 358 Secondly, the slipperiness of the bed can also be sensitive to ice shelf buttressing (Gudmundsson, 2003;
 359 Schoof, 2007). We acknowledge that our inversion method means our slipperiness estimate is fixed in time
 360 and consequently does not allow for regions of low basal drag to migrate inland. Immediately inland of
 361 the final grounding line position lies a section of reverse bed slope that may allow for some accelerated
 362 retreat as the grounding line moves through this region in the future. Errors in bed topography are small
 363 (16 m) compared to ice thickness (~ 700 m: Figure 6) along the region of grounding line retreat in our
 364 experiments. However, between 50 and 60 km along the glacier centerline, errors in bed elevation increase to

365 50 m. Given these uncertainties in bed topography, and the limitations outlined above (i.e. fixed terminus
366 and basal slipperiness) we cannot rule out that the grounding line will retreat further over the next 100
367 years. Crucially, after ~ 60 km (Figure 6a), the bed topography becomes steep ($+1.56^\circ$) and seaward
368 sloping, before flattening out. Thus, if additional forcing in our experiments had forced the grounding line
369 further inland, we do not anticipate a dramatic increase in PG's contribution to sea level rise, as this steep
370 topography would likely prevent runaway retreat of the grounding line. Further work that directly assesses
371 the sensitivity of Petermann Glacier to bed topography and basal sliding is needed.

372 CONCLUSIONS

373 Here, we present the results of three modelling experiments that perturb the extent of the Petermann
374 Glacier ice shelf to explore its sensitivity to various forcings and its dynamic response and potential sea
375 level rise contribution over the next 100 years. Our results have shown that under several scenarios of ice
376 shelf thinning and retreat, unstable rapid retreat of PG's grounding line is unlikely over the next 100 years.
377 Under enhanced basal melt alone, PG will lose 233 Gt of ice, almost 100 Gt more than if current conditions
378 are maintained. Ice loss is greater (313 Gt) if the ice shelf calves away episodically alongside enhanced
379 melt rates, due to a loss of buttressing from the laterally confined portions of the shelf near the grounding
380 line. Immediate collapse of the shelf further increases ice loss to 333 Gt of volume above flotation by 2100,
381 equivalent to 0.92 mm of global mean sea level rise. It appears that glacier geometry is the dominant
382 control on grounding line retreat and the grounding line could stabilize at a rise in bed topography ~ 12 km
383 inland of its current position. This stabilisation could prevent a substantial contribution to global mean
384 sea level rise in response to the loss of the ice shelf. The question still remains as to the future stability
385 of PG if the entire ice shelf collapses, and calving then occurs from a grounded terminus. However, unlike
386 glaciers with former ice shelves elsewhere in Greenland (Zachariæ Isstrøm and Jakobshavn Isbræ), where
387 deep retrograde beds and widening fjords allowed for sustained retreat after ice shelf collapse (Mouginot
388 and others, 2015; Choi and others, 2017; Guo and others, 2019), PG's inland geometry, (steep prograde bed
389 and narrow fjord: Figure 6) does not suggest that grounded ice calving will force rapid unstable retreat in
390 the future. Hence, PG may be geometrically constrained from becoming sensitive to calving in the future.

391 **ACKNOWLEDGEMENTS**

392 This research was funded by a Natural Environment Research Council Doctoral Scholarship (grant number:
393 NE/L002590/1) awarded to E. A. Hill through the IAPETUS Doctoral Training Partnership and Newcastle
394 University, UK. The ice flow model ($\tilde{U}a$) used to conduct this study can be acquired from <http://doi.org/10.5281/zenodo.3706624> (Gudmundsson, 2020). All datasets used to produce the results of this
395 paper are available as follows. The RACMO2.3 Greenland surface mass balance dataset was provided on
396 request by Brice Noël and Michiel van den Broeke, to whom we are grateful. Additional datasets are freely
397 available via the following sources: the Operation IceBridge BedMachine version 3 dataset (Morlighem
398 and others, 2017) available at doi.org/10.5067/2CIX82HUV88Y, and Greenland annual ice sheet velocities
399 (Joughin and others, 2010b) from the MEaSUREs program available at doi.org/10.5067/0C7B04ZM9G6Q.
400 We are grateful to the Editor and two anonymous reviewers for their comments on the manuscript.
401

402 **REFERENCES**

- 403 Åkesson H, Nisancioglu KH and Nick FM (2018) Impact of Fjord Geometry on Grounding Line Stability. *Frontiers*
404 *in Earth Science*, **6**(June), 1–16, ISSN 2296-6463 (doi: 10.3389/feart.2018.00071)
- 405 Bondzio JH, Morlighem M, Seroussi H, Kleiner T, Rückamp M, Mougnot J, Moon T, Larour EY and Humbert A
406 (2017) The mechanisms behind Jakobshavn Isbræ’s acceleration and mass loss: A 3-D thermomechanical model
407 study. *Geophysical Research Letters*, **44**(12), 6252–6260, ISSN 19448007 (doi: 10.1002/2017GL073309)
- 408 Brough S, Carr JR, Ross N and Lea JM (2019) Exceptional retreat of kangerlussuaq glacier, east greenland, between
409 2016 and 2018. *Frontiers in Earth Science*, **7**, 123, ISSN 2296-6463 (doi: 10.3389/feart.2019.00123)
- 410 Bunce C, Carr JR, Nienow PW, Ross N and Killick R (2018) Ice front change of marine-terminating outlet glaciers
411 in northwest and southeast Greenland during the 21st century. *Journal of Glaciology*, 1–13, ISSN 00221430 (doi:
412 10.1017/jog.2018.44)
- 413 Cai C, Rignot E, Menemenlis D and Nakayama Y (2017) Observations and modeling of ocean-induced melt beneath
414 Petermann Glacier Ice Shelf in northwestern Greenland. *Geophysical Research Letters*, **44**(16), 8396–8403, ISSN
415 19448007 (doi: 10.1002/2017GL073711)
- 416 Carr JR, Stokes C and Vieli A (2014) Recent retreat of major outlet glaciers on Novaya Zemlya, Russian Arctic,
417 influenced by fjord geometry and sea-ice conditions. *Journal of Glaciology*, **60**(219), 155–170, ISSN 00221430 (doi:
418 10.3189/2014JoG13J122)

- 419 Catania GA, Stearns LA, Sutherland DA, Fried MJ, Bartholomaus TC, Morlighem M, Shroyer E and Nash J (2018)
420 Geometric Controls on Tidewater Glacier Retreat in Central Western Greenland. *Journal of Geophysical Research:*
421 *Earth Surface*, ISSN 21699003 (doi: 10.1029/2017JF004499)
- 422 Choi Y, Morlighem M, Rignot E, Mouginot J and Wood M (2017) Modeling the Response of Nioghalvfjærdsfjorden
423 and Zachariae Isstrøm Glaciers, Greenland, to Ocean Forcing Over the Next Century. *Geophysical Research Letters*,
424 **44**(21), 071–11, ISSN 19448007 (doi: 10.1002/2017GL075174)
- 425 Cornford SL, Martin DF, Graves DT, Ranken DF, Le Brocq AM, Gladstone RM, Payne AJ, Ng EG and Lipscomb
426 WH (2013) Adaptive mesh, finite volume modeling of marine ice sheets. *Journal of Computational Physics*, **232**(1),
427 529–549
- 428 De Rydt J, Gudmundsson GH, Rott H and Bamber JL (2015) Modeling the instantaneous response of glaciers after
429 the collapse of the Larsen B Ice Shelf. *Geophysical Research Letters*, **42**(13), 5355–5363, ISSN 19448007 (doi:
430 10.1002/2015GL064355)
- 431 Durand G, Gagliardini O, Zwinger T, Meur EL and Hindmarsh RC (2009) Full Stokes modeling of marine
432 ice sheets: Influence of the grid size. *Annals of Glaciology*, **50**(52), 109–114, ISSN 02603055 (doi: 10.3189/
433 172756409789624283)
- 434 Engwirda D (2014) Locally optimal Delaunay-refinement and optimisation-based mesh generation. In *Ph.D Thesis*,
435 School of Mathematics and Statistics, University of Sydney
- 436 Favier L, Durand G, Cornford SL, Gudmundsson GH, Gagliardini O, Gillet-Chaulet F, Zwinger T, Payne AJ and
437 Le Brocq AM (2014) Retreat of Pine Island Glacier controlled by marine ice-sheet instability. *Nature Climate*
438 *Change*, **4**(2), 117–121, ISSN 1758678X (doi: 10.1038/nclimate2094)
- 439 Glen JW (1955) The creep of polycrystalline ice. *Proceedings of the Royal Society of London. Series A. Mathematical*
440 *and Physical Sciences*, **228**(1175), 519–538
- 441 Goldberg D, Holland DM and Schoof C (2009) Grounding line movement and ice shelf buttressing in marine ice
442 sheets. *Journal of Geophysical Research: Earth Surface*, **114**(4), ISSN 21699011 (doi: 10.1029/2008JF001227)
- 443 Gudmundsson GH (2003) Transmission of basal variability to a glacier surface. *Journal of Geophysical Research:*
444 *Solid Earth*, **108**(B5), 1–19 (doi: 10.1029/2002jb002107)
- 445 Gudmundsson GH (2013) Ice-shelf buttressing and the stability of marine ice sheets. *Cryosphere*, **7**(2), 647–655, ISSN
446 19940424 (doi: 10.5194/tc-7-647-2013)
- 447 Gudmundsson GH (2020) Ghilmarg/uasource: Ua2019b (version v2019b) (doi: 10.5281/zenodo.3706624)

- 448 Gudmundsson GH, Krug J, Durand G, Favier L and Gagliardini O (2012) The stability of grounding lines on
449 retrograde slopes. *Cryosphere*, **6**(6), 1497–1505, ISSN 19940416 (doi: 10.5194/tc-6-1497-2012)
- 450 Gudmundsson GH, Paolo FS, Adusumilli S and Fricker HA (2019) Instantaneous antarctic ice sheet mass loss driven
451 by thinning ice shelves. *Geophysical Research Letters*, **46**(23), 13903–13909 (doi: 10.1029/2019GL085027)
- 452 Guo X, Zhao L, Gladstone RM, Sun S and Moore JC (2019) Simulated retreat of jakobshavn isbræ during the 21st
453 century. *The Cryosphere*, **13**(11), 3139–3153 (doi: 10.5194/tc-13-3139-2019)
- 454 Haseloff M and Sergienko OV (2018) The effect of buttressing on grounding line dynamics. *Journal of Glaciology*,
455 **64**(245), 417–431, ISSN 00221430 (doi: 10.1017/jog.2018.30)
- 456 Hill EA, Carr JR and Stokes CR (2017) A Review of Recent Changes in Major Marine-Terminating Outlet Glaciers
457 in Northern Greenland. *Frontiers in Earth Science*, **4**(111), 1–23, ISSN 2296-6463 (doi: 10.3389/feart.2016.00111)
- 458 Hill EA, Carr JR, Stokes CR and Gudmundsson GH (2018a) Dynamic changes in outlet glaciers in northern Greenland
459 from 1948 to 2015. *The Cryosphere*, **12**, 3243–3263, ISSN 1994-0440 (doi: 10.5194/tc-12-3243-2018)
- 460 Hill EA, Gudmundsson GH, Carr JR and Stokes CR (2018b) Velocity response of Petermann Glacier , northwest
461 Greenland , to past and future calving events. *Cryosphere*, **12**(12), 3907–3921, ISSN 19940424 (doi: 10.5194/
462 tc-12-3907-2018)
- 463 Hogg AE, Shepherd A, Gourmelen N and Engdahl M (2016) Grounding line migration from 1992 to 2011 on
464 Petermann Glacier, North-West Greenland. *Journal of Glaciology*, **62**(236), 1104–1114, ISSN 00221430 (doi:
465 10.1017/jog.2016.83)
- 466 Howat IM, Joughin I and Scambos TA (2007) Rapid changes in ice discharge from Greenland outlet glaciers. *Science*,
467 **315**(5818), 1559–1561, ISSN 00368075 (doi: 10.1126/science.1138478)
- 468 Jakobsson M, Hogan KA, Mayer LA, Mix A, Jennings A, Stoner J, Eriksson B, Jerram K, Mohammad R, Pearce C,
469 Reilly B and Stranne C (2018) The Holocene retreat dynamics and stability of Petermann Glacier in northwest
470 Greenland. *Nature Communications*, **9**(1), ISSN 20411723 (doi: 10.1038/s41467-018-04573-2)
- 471 Jamieson SSR, Vieli A, Livingstone SJ, O’Cofaigh C, Stokes CR, Hillenbrand CD and Dowdeswell JA (2012) Ice-
472 stream stability on a reverse bed slope. *Nature Geoscience*, **5**(11), 799–802, ISSN 1752-0894 (doi: 10.1038/
473 NGE01600)
- 474 Jamieson SSR, Vieli A, Ó Cofaigh C, Stokes CR, Livingstone SJ and Hillenbrand CD (2014) Understanding controls
475 on rapid ice-stream retreat during the last deglaciation of marguerite bay, antarctica, using a numerical model.
476 *Journal of Geophysical Research: Earth Surface*, **119**(2), 247–263 (doi: 10.1002/2013JF002934)

- 477 Johannessen OM, Babiker M and Miles MW (2013) Unprecedented Retreat in a 50-Year Observational Record for
478 Petermann. *Atmospheric and Oceanic Science Letters*, **6**(5), 259–265 (doi: 10.3878/j.issn.1674-2834.13.0021)
- 479 Johnson HL, Münchow A, Falkner KK and Melling H (2011) Ocean circulation and properties in Petermann Fjord,
480 Greenland. *Journal of Geophysical Research: Oceans*, **116**(1), 1–18, ISSN 21699291 (doi: 10.1029/2010JC006519)
- 481 Joughin I, Abdalati W and Fahnestock Ma (2004) Large fluctuations in speed on Greenland’s Jakobshavn Isbrae
482 glacier. *Nature*, **432**, 608–610, ISSN 0028-0836 (doi: 10.1038/nature03130)
- 483 Joughin I, Howat IM, Fahnestock M, Smith B, Krabill W, Alley RB, Stern H and Truffer M (2008) Continued evolution
484 of Jakobshavn Isbrae following its rapid speedup. *Journal of Geophysical Research: Earth Surface*, **113**(4), 1–14
485 (doi: 10.1029/2008JF001023)
- 486 Joughin I, Smith BE and Holland DM (2010a) Sensitivity of 21st century sea level to ocean-induced thinning of pine
487 island glacier, antarctica. *Geophysical Research Letters*, **37**(20) (doi: 10.1029/2010GL044819)
- 488 Joughin I, Smith BE, Howat IM, Scambos T and Moon T (2010b) Greenland flow variability from ice-sheet-wide
489 velocity mapping. *Journal of Glaciology*, **56**(197), 415–430, ISSN 00221430 (doi: 10.3189/002214310792447734)
- 490 Joughin I, Smith BE, Shean DE and Floricioiu D (2014) Brief communication: Further summer speedup of jakobshavn
491 isbræ. *The Cryosphere*, **8**(1), 209–214 (doi: 10.5194/tc-8-209-2014)
- 492 MacAyeal DR (1989) Large-scale ice flow over a viscous basal sediment: Theory and application to ice stream B,
493 Antarctica. *Journal of Geophysical Research: Solid Earth*, **94**(B4), 4071–4087, ISSN 01480227 (doi: 10.1029/
494 JB094iB04p04071)
- 495 Miles B, Stokes C and Jamieson S (2018) Velocity increases at Cook Glacier, East Antarctica, linked to ice shelf loss
496 and a subglacial flood event. *Cryosphere*, **12**(10), 3123–3136, ISSN 19940424 (doi: 10.5194/tc-12-3123-2018)
- 497 Moon T, Joughin I, Smith B and Howat I (2012) 21st-century evolution of Greenland outlet glacier velocities. *Science*,
498 **336**(6081), 576–578, ISSN 10959203 (doi: 10.1126/science.1219985)
- 499 Morland LW (1987) Unconfined Ice-Shelf Flow. In CJ der Veen and J Oerlemans (eds.), *Dynamics of the*
500 *West Antarctic Ice Sheet*, 99–116, Springer Netherlands, Dordrecht, ISBN 978-94-009-3745-1 (doi: 10.1007/
501 978-94-009-3745-1{_}6)
- 502 Morlighem M, Williams CN, Rignot E, An L, Arndt JE, Bamber JL, Catania G, Chauché N, Dowdeswell JA, Dorschel
503 B, Fenty I, Hogan K, Howat I, Hubbard A, Jakobsson M, Jordan TM, Kjeldsen KK, Millan R, Mayer L, Mouginot
504 J, Noël BP, O’Cofaigh C, Palmer S, Rysgaard S, Seroussi H, Siegert MJ, Slabon P, Straneo F, van den Broeke
505 MR, Weinrebe W, Wood M and Zinglensen KB (2017) BedMachine v3: Complete Bed Topography and Ocean

- 506 Bathymetry Mapping of Greenland From Multibeam Echo Sounding Combined With Mass Conservation. *Geo-*
507 *physical Research Letters*, **44**(21), 051–11, ISSN 19448007 (doi: 10.1002/2017GL074954)
- 508 Mouginit J, Rignot E, Scheuchl B, Fenty I, Khazendar A, Morlighem M, Buzzi A and Paden J (2015) Fast retreat of
509 Zachariæ Isstrøm, northeast Greenland. *Science*, **350**, 1357–1361, ISSN 0036-8075 (doi: 10.1126/science.aac7111)
- 510 Münchow A, Falkner K, Melling H, Rabe B and Johnson H (2011) Ocean Warming of Nares Strait Bottom Waters off
511 Northwest Greenland, 2003–2009. *Oceanography*, **24**(3), 114–123, ISSN 10428275 (doi: 10.5670/oceanog.2011.62)
- 512 Münchow A, Padman L and Fricker HA (2014) Interannual changes of the floating ice shelf of Petermann Gletscher,
513 North Greenland, from 2000 to 2012. *Journal of Glaciology*, **60**(221), 489–499, ISSN 00221430 (doi: 10.3189/
514 2014JoG13J135)
- 515 Münchow A, Padman L, Washam P and Nicholls K (2016) The Ice Shelf of Petermann Gletscher, North Greenland,
516 and Its Connection to the Arctic and Atlantic Oceans. *Oceanography*, **29**(4), 84–95, ISSN 10428275 (doi: 10.5670/
517 oceanog.2016.101)
- 518 Nick FM, Vieli A, Howat IM and Joughin I (2009) Large-scale changes in Greenland outlet glacier dynamics triggered
519 at the terminus. *Nature Geoscience*, **2**(2), 110–114, ISSN 1752-0894 (doi: 10.1038/ngeo394)
- 520 Nick FM, Van Der Veen CJ, Vieli A and Benn DI (2010) A physically based calving model applied to marine outlet
521 glaciers and implications for the glacier dynamics. *Journal of Glaciology*, **56**(199), 781–794, ISSN 00221430 (doi:
522 10.3189/002214310794457344)
- 523 Nick FM, Luckman A, Vieli A, Van Der Veen CJ, Van As D, Van De Wal RSW, Pattyn F, Hubbard AL and
524 Floricioiu D (2012) The response of Petermann Glacier, Greenland, to large calving events, and its future stability
525 in the context of atmospheric and oceanic warming. *Journal of Glaciology*, **58**(208), 229–239, ISSN 00221430 (doi:
526 10.3189/2012JoG11J242)
- 527 Nick FM, Vieli A, Andersen ML, Joughin I, Payne A, Edwards TL, Pattyn F and Van De Wal RSW (2013) Future
528 sea-level rise from Greenland’s main outlet glaciers in a warming climate. *Nature*, **497**(7448), 235–238, ISSN
529 1476-4687 (doi: 10.1038/nature12068)
- 530 Noël B, Jan Van De Berg W, MacHguth H, Lhermitte S, Howat I, Fettweis X and Van Den Broeke MR (2016) A
531 daily, 1 km resolution data set of downscaled Greenland ice sheet surface mass balance (1958-2015). *Cryosphere*,
532 **10**(5), 2361–2377, ISSN 19940424 (doi: 10.5194/tc-10-2361-2016)
- 533 Paolo FS, Fricker HA and Padman L (2015) Volume loss from Antarctic ice shelves is accelerating. *Science*, **348**(6232),
534 327–331, ISSN 10959203 (doi: 10.1126/science.aaa0940)

- 535 Pattyn F, Schoof C, Perichon L, Hindmarsh RC, Bueler E, De Fleurian B, Durand G, Gagliardini O, Gladstone R,
536 Goldberg D, Gudmundsson GH, Huybrechts P, Lee V, Nick FM, Payne AJ, Pollard D, Rybak O, Saito F and Vieli
537 A (2012) Results of the marine ice sheet model intercomparison project, MISMIP. *Cryosphere*, **6**(3), 573–588,
538 ISSN 19940416 (doi: 10.5194/tc-6-573-2012)
- 539 Reese R, Gudmundsson GH, Levermann A and Winkelmann R (2018a) The far reach of ice-shelf thinning in Antarc-
540 tica. *Nature Climate Change*, **8**(January), ISSN 1758-678X (doi: 10.1038/s41558-017-0020-x)
- 541 Reese R, Winkelmann R and Gudmundsson GH (2018b) Grounding-line flux formula applied as a flux condition in
542 numerical simulations fails for buttressed Antarctic ice streams. *The Cryosphere*, **12**, 3229–3242, ISSN 1994-0440
543 (doi: 10.5194/tc-12-3229-2018)
- 544 Rignot E and Steffen K (2008) Channelized bottom melting and stability of floating ice shelves. *Geophysical Research*
545 *Letters*, **35**(2), 2–6, ISSN 00948276 (doi: 10.1029/2007GL031765)
- 546 Rignot E, Box JE, Burgess E and Hanna E (2008) Mass balance of the Greenland ice sheet from 1958 to 2007.
547 *Geophysical Research Letters*, **35**(20), 1–5, ISSN 00948276 (doi: 10.1029/2008GL035417)
- 548 Rignot E, Mouginot J, Morlighem M, Seroussi H and Scheuchl B (2014) Widespread, rapid grounding line retreat of
549 pine island, thwaites, smith, and kohler glaciers, west antarctica, from 1992 to 2011. *Geophysical Research Letters*,
550 **41**(10), 3502–3509 (doi: 10.1002/2014GL060140)
- 551 Rückamp M, Neckel N, Berger S, Humbert A and Helm V (2019) Calving Induced Speedup of Petermann Glacier.
552 *Journal of Geophysical Research: Earth Surface*, **124**(1), 216–228, ISSN 21699011 (doi: 10.1029/2018JF004775)
- 553 Scambos TA, Bohlander JA, Shuman CA and Skvarca P (2004) Glacier acceleration and thinning after ice shelf
554 collapse in the Larsen B embayment, Antarctica. *Geophysical Research Letters*, **31**(18), 2001–2004, ISSN 00948276
555 (doi: 10.1029/2004GL020670)
- 556 Schoof C (2007) Ice sheet grounding line dynamics: Steady states, stability, and hysteresis. *Journal of Geophysical*
557 *Research: Earth Surface*, **112**(3), 1–19, ISSN 21699011 (doi: 10.1029/2006JF000664)
- 558 Schoof C, Davis AD and Popa TV (2017) Boundary layer models for calving marine outlet glaciers. *Cryosphere*,
559 **11**(5), 2283–2303, ISSN 19940424 (doi: 10.5194/tc-11-2283-2017)
- 560 Seroussi H and Morlighem M (2018) Representation of basal melting at the grounding line in ice flow models. *The*
561 *Cryosphere*, **12**(10), 3085–3096 (doi: 10.5194/tc-12-3085-2018)
- 562 Shroyer EL, Padman L, Samelson RM, Münchow A and Stearns LA (2017) Seasonal control of Petermann Gletscher
563 ice-shelf melt by the ocean’s response to sea-ice cover in Nares Strait. *Journal of Glaciology*, **63**(238), 324–330,
564 ISSN 00221430 (doi: 10.1017/jog.2016.140)

- 565 Simonsen SB and Sørensen LS (2017) Implications of changing scattering properties on Greenland ice sheet volume
566 change from Cryosat-2 altimetry. *Remote Sensing of Environment*, **190**, 207–216, ISSN 00344257 (doi: 10.1016/j.
567 rse.2016.12.012)
- 568 Steiger N, Nisancioglu KH, Åkesson H, De Fleurian B and Nick FM (2017) Non-linear retreat of Jakobshavn Isbrae
569 since the Little Ice Age controlled by geometry. *The Cryosphere*, **1**(September), 1–27, ISSN 1994-0424 (doi:
570 10.5194/tc-2017-151)
- 571 Stokes CR, Corner GD, Winsborrow MCM, Husum K and Andreassen K (2014) Asynchronous response of marine-
572 terminating outlet glaciers during deglaciation of the Fennoscandian ice sheet. *Geology*, **42**(5), 455–458, ISSN
573 19432682 (doi: 10.1130/G35299.1)
- 574 Thomas R (2004) Force perturbation analysis of recent thinning and acceleration of Jakobshavn Isbrae, Greenland.
575 *Journal of Glaciology*, **50**(168), 57–66, ISSN 00221430 (doi: 10.3189/172756504781830321)
- 576 Washam P, Münchow A and Nicholls KW (2018) A Decade of Ocean Changes Impacting the Ice Shelf of Pe-
577 termann Gletscher, Greenland. *Journal of Physical Oceanography*, **48**(10), 2477–2493, ISSN 0022-3670 (doi:
578 10.1175/JPO-D-17-0181.1)
- 579 Weertman J (1957) On the sliding of glaciers. *Journal of glaciology*, **3**(21), 33–38
- 580 Wilson N, Straneo F and Heimbach P (2017) Satellite-derived submarine melt rates and mass balance (2011-
581 2015) for Greenland’s largest remaining ice tongues. *Cryosphere*, **11**(6), 2773–2782, ISSN 19940424 (doi:
582 10.5194/tc-11-2773-2017)